[AMERICAN JOURNAL OF SCIENCE, VOL. 296, JUNE, 1996, P. 633–663]

CONTROLS ON THE PYRITIZATION OF EXCEPTIONALLY PRESERVED FOSSILS: AN ANALYSIS OF THE LOWER DEVONIAN HUNSRÜCK SLATE OF GERMANY

D. E. G. BRIGGS*, R. RAISWELL**, S. H. BOTTRELL**, D. HATFIELD**, and C. BARTELS***

ABSTRACT. Sulfur isotope and C-S-Fe elemental data from the Lower Devonian (Siegenian/Emsian) Hunsrück Slate of Germany allow the conditions that led to the pyritization of soft-bodied fossils to be determined. The slates preserving pyritized soft-tissues generally contain low concentrations of organic matter (0.3-0.4 percent C) and pyrite sulfur (0-0.2 percent S) respectively but are unusually rich in total and HCl-extractable iron (concentrations of iron are significantly lower in samples of the Hunsrück Slate from areas where fossils lack pyritized soft-tissues). The fossil pyrite is very enriched in ^{34}S compared to fine-grained, disseminated pyrite in the adjacent slates ($\Delta_{fossil-sediment}$ = 10 to 50 permil), suggesting that pyritization of the fossils persisted into later stages of authigenic mineralization. Pyrite formation in the sediments was limited by the low concentrations of metabolisable organic matter, leaving residual sulfate and iron available for continued fossil pyritization in organic-rich microenvironments. A diffusion-with-precipitation model indicates that a critical control on the initial preservation of readily metabolisable soft tissue in this way is the presence of high concentrations of sediment iron capable of being solubilized during shallow burial diagenesis in association with low concentrations of metabolisable organic matter in the matrix. Pore waters rich in dissolved iron allow the sulfide generated by the decay of readily metabolisable soft tissue to be trapped efficiently within the carcass.

INTRODUCTION

Fossils that preserve more than biomineralized skeletons (that is, shells, bones, teeth) are a fundamental source of data on the history of life (see Briggs, 1991). Decay-resistant tissues, such as cuticles, may survive to be transformed by diagenesis into organic macromolecules that persist in sedimentary rocks (Baas and others 1995; Briggs and others 1995). More labile tissues, like muscle, however, which are broken down readily by microbial processes, are normally only preserved as a result of early replacement by inorganic minerals. A number of authigenic minerals may perform this function (see Allison, 1988). Calcium phosphate yields the highest fidelity, three-dimensional preservation (Briggs and others, 1993; Martill, 1990). Phosphatized soft-tissues are relatively widespread in the fossil record, and the process has been duplicated under experimen-

* Department of Geology, University of Bristol, Wills Memorial Building, Queen's Road, Bristol BS8 1RJ, United Kingdom.

** Department of Earth Sciences, University of Leeds, Leeds LS2 9JT, United Kingdom.

*** Deutsches Bergbau-Museum, Am Bergbaumuseum 28, D-4630 Bochum 1, Germany.

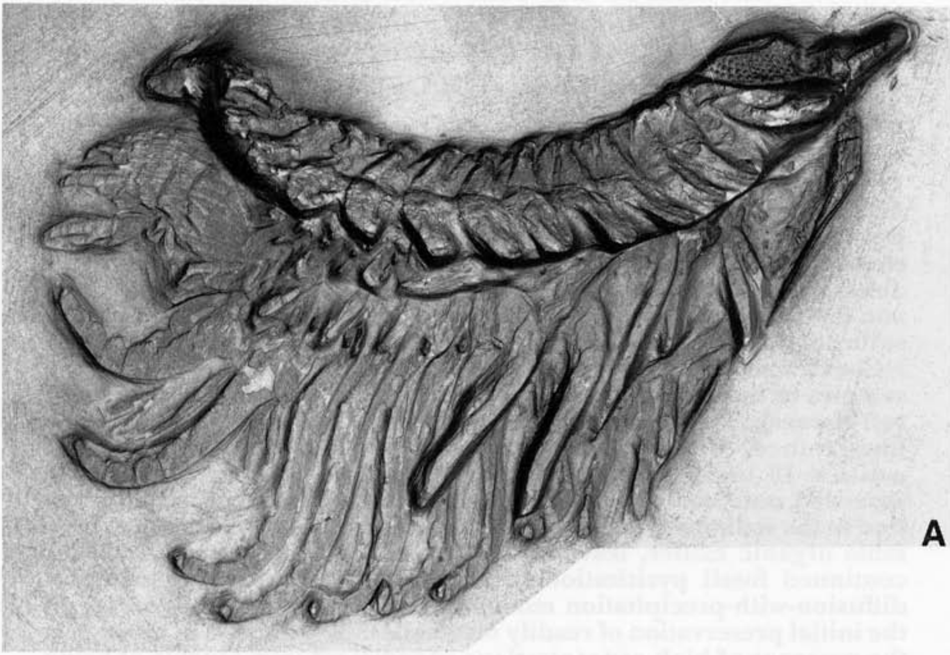

Fig. 1. Examples of the trilobite *Chotecops* sp. from the Eschenbach-Bocksberg quarry, Bundenbach. (A) Right lateral view with the appendages extending below the exoskeleton (HS 214) (×1.0).

tal conditions in the laboratory (Briggs and Kear, 1993; Briggs and others, 1993; Hof and Briggs, 1997). In contrast, pyrite, in spite of its ubiquity in fine-grained marine sediments and common occurrence in association with shelly fossils (Hudson, 1982), is rarely associated with the preservation of soft tissues (Allison and Briggs, 1991). The Devonian Hunsrück Slate of Germany and Beecher's Trilobite Bed in the Upper Ordovician of New York State (Briggs, Bottrell, and Raiswell, 1991) are the only extensive examples of soft-part pyritization. (Recent work (Wilby, Briggs, and Riou, in review) has shown that pyrite is also important in the preservation of soft-tissues in the Jurassic of La Voulte-sur-Rhône, France, but there its source may be hydrothermal.) Here we employ a variety of geochemical methods to explore the reasons for the rarity of pyritized soft-tissues. Such investigations have important implications for our understanding of authigenic mineral growth in sediments.

The pyritized fossils of the Devonian Hunsrück Slate of western Germany (Stürmer, Schaarschmidt, and Mittmeyer, 1980; Kott and Wuttke, 1987; Bartels and Brassel, 1990; Bartels and Wuttke, 1994a) include a diverse biota of abundant trilobites (fig. 1A, C) (Stürmer and Bergström, 1973) and other arthropods, echinoderms (fig. 2), fish,

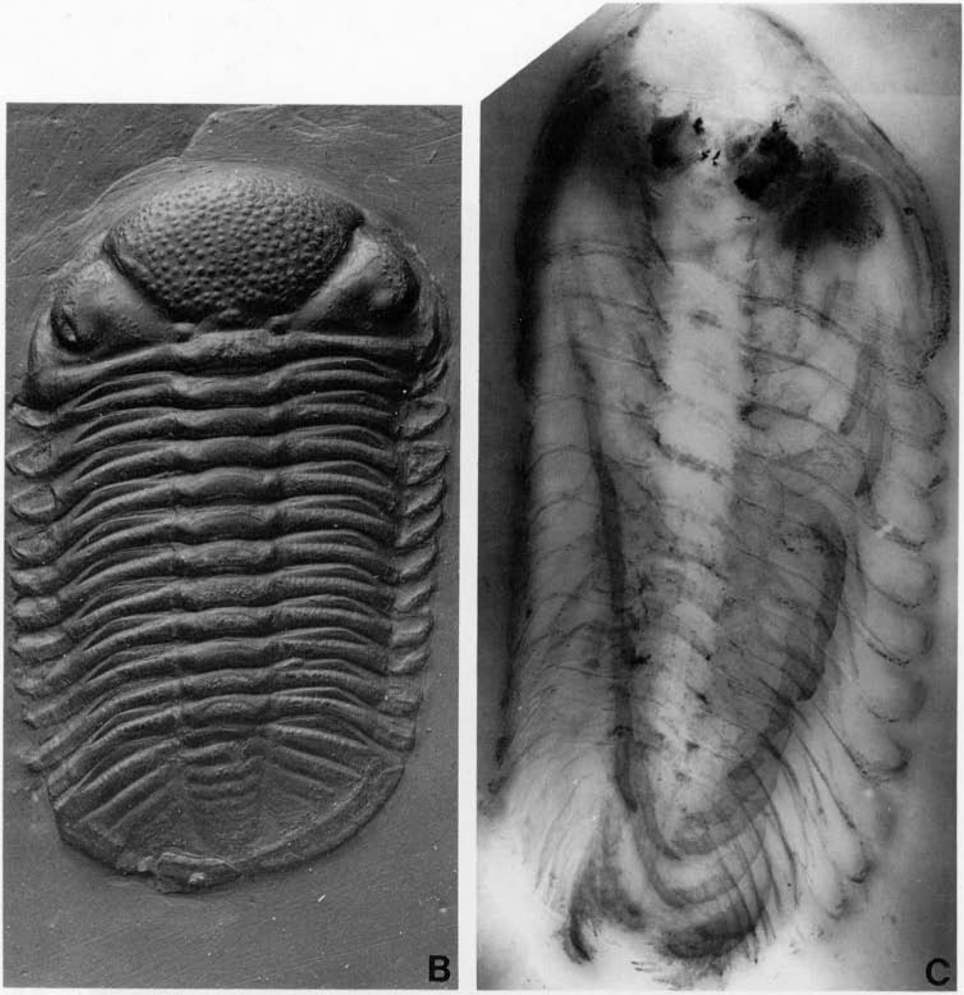

Fig. 1(B) Dorsal view of an unpyritized specimen (HS 718) (×1.25). (C) X-radiograph showing traces of the stomach in the head region, and the appendages (Stürmer WS4171, magnification unknown). A, B. Specimens from the Bartels Collection, Deutsches Bergbau-Museum.

cephalopods (Stürmer, 1985), and other groups. While some of the interpretations of soft-part morphology in the Hunsrück Slate fossils may be problematic (Otto, 1994; but see Bartels and Wuttke, 1994b; Bartels and Blind, 1995), it is clear that a range of non-biomineralized structures is preserved. These include the limbs of arthropods (fig. 1A, C) and the granular skin that connects the arms of some ophiuroids (fig. 2A). Specimens have traditionally been prepared using blades and needles

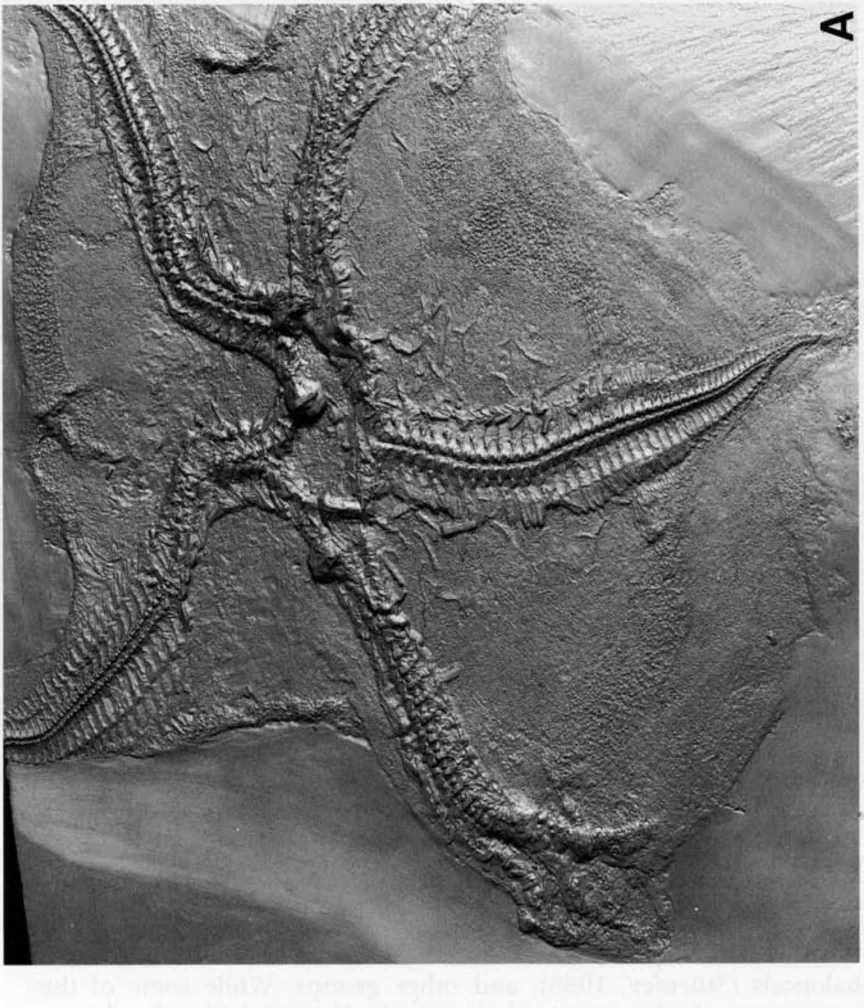

Fig. 2. Ophiuroids from the Eschenbach-Bocksberg mine, Bundenbach. A. *Cheiropteraster giganteus* showing the granular skin between the arms (×0.6).

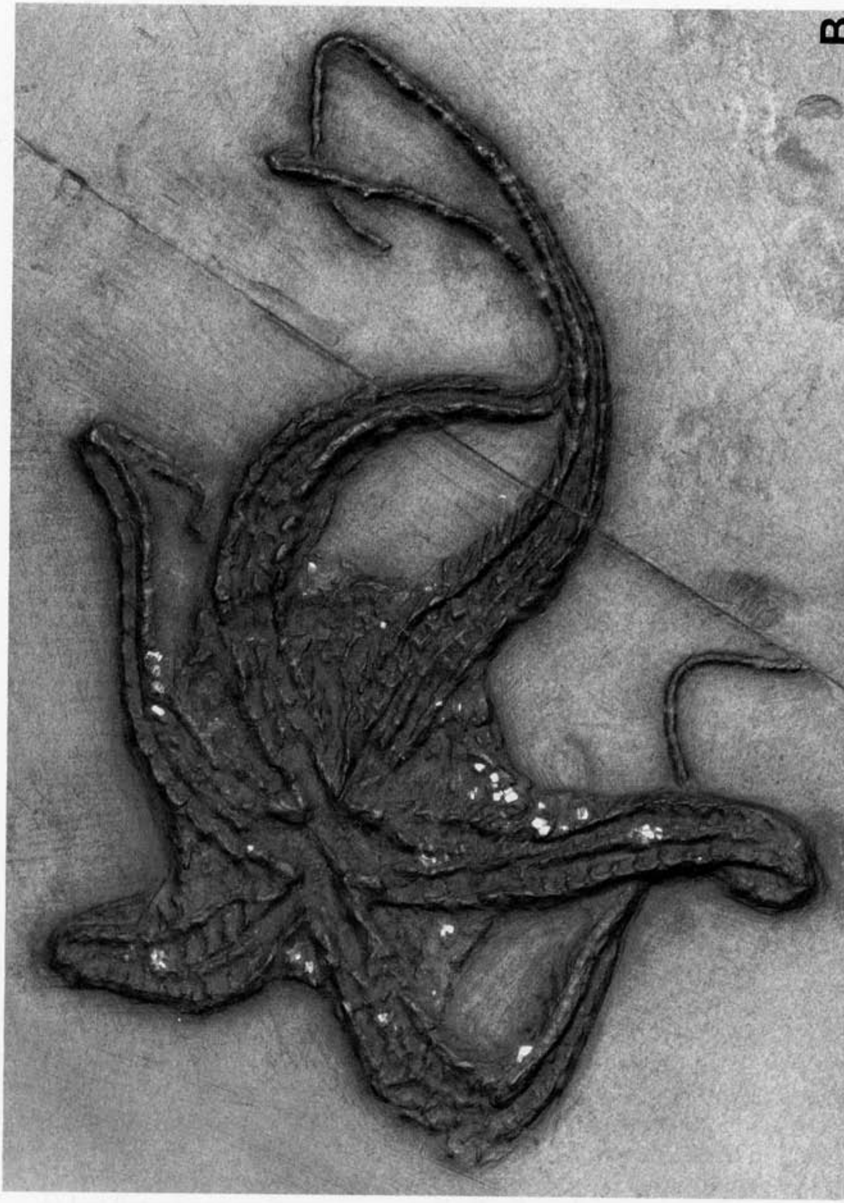

Fig. 2. B. *Taeniaster beneckei*, an unusual individual with six arms and late euhedral crystals of pyrite present on the surface (HS 164) (×2.2). Specimens from the Bartels Collection, Deutsches Bergbau-Museum.

(fig. 1A) exploiting the greater resistance of pyrite compared to slate matrix. Recently spectacular preparations of delicate pyritized features like echinoderm skin (fig. 2A) have been effected (by CB) using a specially constructed airbrasive machine and iron powder. Study of the fossils is also facilitated by X-radiography (Stürmer, Schaarschmidt, and Mittmeyer, 1980) which reveals pyritized structures concealed within the slate matrix (fig. 1C).

The trilobites from Beecher's Trilobite Bed are one of the very few examples of fossil pyritization that have been studied using sulfur isotopes to determine the paragenesis of fossil and matrix pyrite (Briggs, Bottrell, and Raiswell, 1991; see also Beier and Feldman, 1991; Hudson, 1982; Fisher and Hudson, 1985). Beecher's Trilobite Bed is a layer ~4 cm thick in the Frankfort Shale dominated by the trilobite *Triarthrus* (Cisne, 1973; Briggs and Edgecombe, 1992). The isotopic geochemistry of the section in the Frankfort Shale including Beecher's Bed reveals a substantial enrichment in ^{34}S at the level containing the trilobites relative to the adjacent beds (Briggs, Bottrell, and Raiswell, 1991). Here we extend the application of sulfur isotope analysis to a wider range of taxa in the Hunsrück Slate. A model for pyritization based on the diffusion-with-precipitation model of Canfield and Raiswell (1991) and Raiswell and others (1993) is utilized to explain soft-tissue preservation and to relate it to sediment iron content.

GEOLOGICAL SETTING OF THE HUNSRÜCK SLATE FOSSILS

The Hunsrück Slate crops out in a belt some 150 km long centered on the Hunsrück area but extending to the north of the Moselle and to the east of the Rhine (fig. 3). It ranges in age from latest Siegenian to mid-Early Emsian. The thickness of the Hunsrück Slate varies with the topography of the basin. It reaches a maximum of about 3000 m (Dittmar, 1995) of which about 1000 m contain roofslates (Bartels and Brassel, 1990) and thins northward where it passes into the Rhenisches Normalfazies. Water depth in the basin was variable but did not greatly exceed 200 m (Mittmeyer, 1980). The classic lithology is a laminated mudstone, with rare lenses of fine sand a few centimeters to several tens of centimeters thick. The neogenesis of chlorite and mica and the growth of chlorite muscovite porphyroblasts (Talbot, 1964; Roy, 1978) indicate that metamorphism attained upper anchizone or lowest greenschist facies conditions, transforming the mudstones to slates. The great majority of the Hunsrück Slate fossils have been collected during the production of roofing slates in areas where mudstone beds of uniform thickness are cleaved parallel to bedding. The mudstones grade laterally into the sandier Rhenish facies to the northwest and to the southeast indicating shallowing in these directions.

In the past up to 600 different mines and quarries produced roofing slate, but significant examples of soft-tissue preservation are restricted to four thin roof-slate horizons in the area around Gemünden and Bundenbach (fig. 4). Thus although two mines (Katzenberg and Margareta near

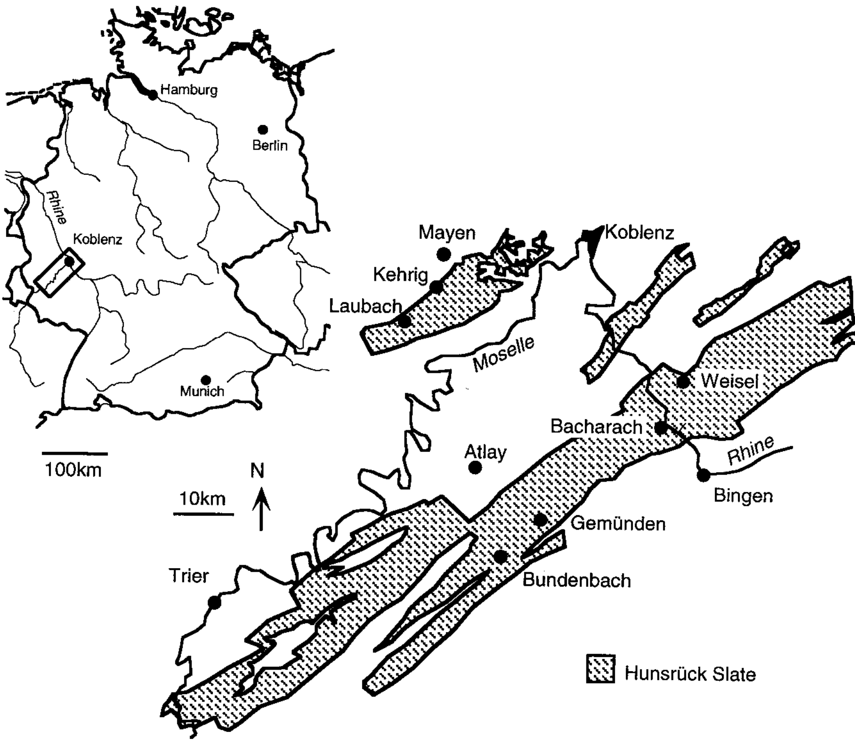

Fig. 3. Map showing the area of Hunsrück Slate outcrop.

Mayen) and three quarries (Atlay, Bacharach, Bundenbach) are still in operation only one, the quarry at Eschenbach-Bocksberg near Bundenbach, is a source of new pyritized fossils. They are very rare; tons of slate may be worked without finding a single well preserved specimen (Bartels and Brassel, 1990). The faunal content of the Hunsrück Slates varies from area to area; asteroids and ophiuroids, for example, are confined essentially to the vicinity of Bundenbach (Bartels and Brassel, 1990). It is clear in many cases that the fauna was buried in situ or transported only a minimal distance. Crinoids are often preserved rooted in the sediment or attached to shells. Horizons with surface trails of trilobites and other arthropods indicate that the bottom was oxygenated. The frequent preservation of laminations indicates that the sediment usually did not support an infauna. At some levels, however, *Chondrites* is common (for example, in the Eschenbach-Bocksberg quarry), which is thought to be indicative of low oxygen levels (Bromley and Ekdale, 1984). The fossils are buried in a variety of attitudes to bedding indicating deposition from a turbulent cloud of sediment (Stürmer and Bergström, 1973). The patchy distribution of the exceptionally preserved fossils may reflect

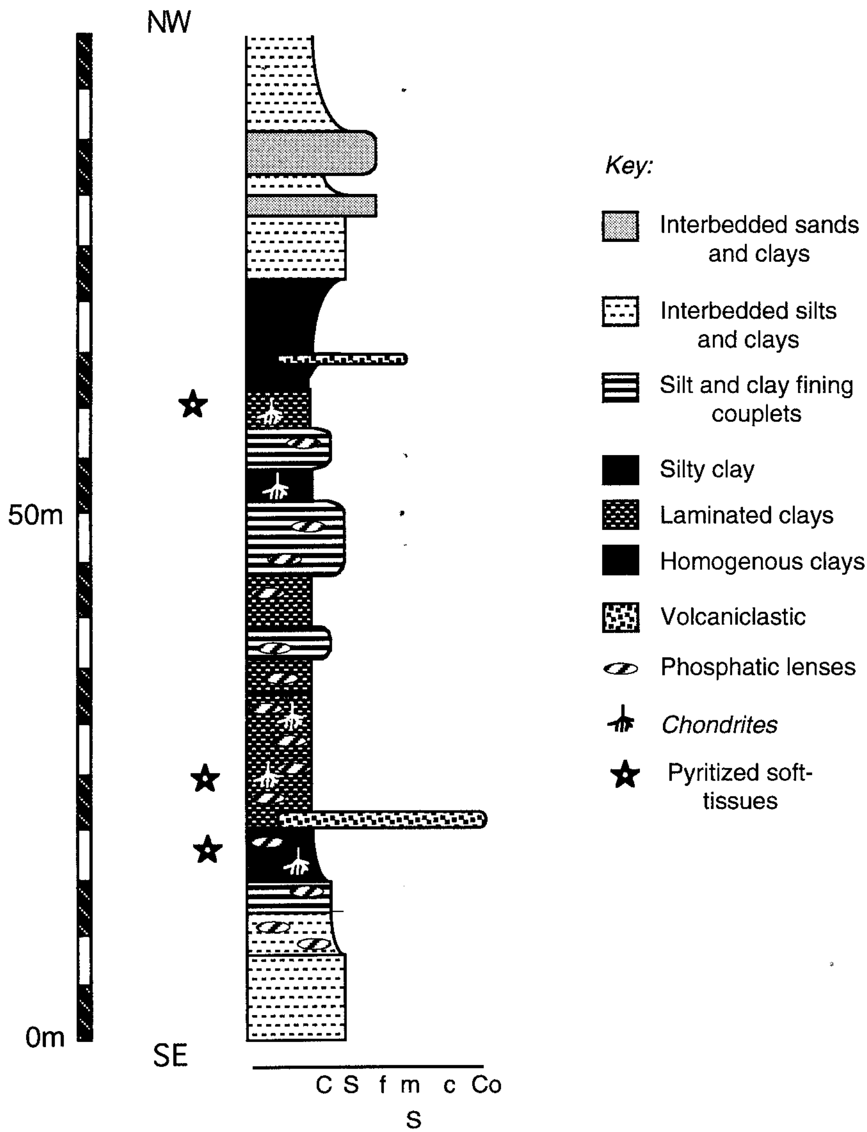

Fig. 4. Sedimentary log (by O. E. Sutcliffe) of the lower part of the Eschenberg-Bocksberg Quarry near Bundenbach showing the section exposed in 1994. The lower three levels that yield exceptionally preserved pyritized fossils are indicated. The fourth lies above the top of the section illustrated.

rapid burial by sediment transported by episodic density-currents into low lying areas on the seafloor (Bartels and Brassel, 1990). Beyond the thin horizons that produce pyritized fossils in the vicinity of Gemünden and Bundenbach other parts of the Hunsrück Slate yield well preserved fossils that are not pyritized (fig. 1B). They lack evidence of the soft-tissues and are usually associated with dark phosphatic material.

SAMPLING AND METHODS

All the pyritized specimens analyzed in conjunction with the present study were collected from the Eschenbach-Bocksberg quarry near Bundenbach. They came from the lower three levels that yield specimens with pyritized soft parts (fig. 4). Because of their rarity and the nature of the quarry it is impossible to excavate for pyritized fossils. Specimens are found as the slate is split during commercial production, and they are accumulated in small numbers by the workers over a long period. Occasionally they can be found on the tips where waste rock is dumped. Thus the precise levels from which the fossils analyzed here came are unknown. A few of the more common pyritized fossils were collected on the tips specifically for this study, but most had been accumulated (by CB) over a period of years. Three unpyritized fossils from other levels in the Eschenbach-Bocksberg quarry (see fig. 1B) and one from the Kreuzberg roofslate mine near Weisel were included as a control (app. 1). Samples of pyrite from the pyritized fossils were removed from different parts (app. 1) by chipping them off with a modified dental drill. Mineral textures were examined with the SEM. The unpyritized fossils were sampled by cutting a piece out of the specimen including the thickness of slate (split as finely as possible) in which it occurred. Thus some matrix above, below, and within the margins of the fossil may have been included. Samples were sawn out of the slates adjacent to the fossils (both pyritized and unpyritized) at radial distances of 1 to 3, 4 to 6, and 10 to 12 cm from the edge of the specimen. Additionally, a block about 15 cm thick was collected to provide a lithological sequence including a lens of pyrite. The lens is tube shaped with the long axis (190 cm) lying parallel to the bedding. The cross section (perpendicular to the bedding) is elliptical with dimensions 4 by 2 cm. The lens is composed of fine-grained crystalline pyrite and quartz but includes no recognizable fossil material. Finally supplementary matrix samples from 10 slabs with complete fossils from areas of the Hunsrück Slate where pyritization does not occur (5 additional specimens from Kreuzberg, 2 from the Maria Schacht mine near Laubach, 2 from the Margaretha mine near Mayen, and 1 from the Bausberg II mine near Kehrig: fig. 3, app. 2) were analyzed to allow a comparison with iron concentrations in association with pyritized specimens. All samples were collected from newly quarried slate and have not been affected by weathering.

Sulfur from pyrite was selectively extracted using the chromous chloride reduction method (Canfield and others, 1986; Newton and others, 1995); H_2S evolved was precipitated as CuS from a standardized copper solution and was subsequently back-titrated with EDTA to determine Cu consumed, and hence pyrite sulfur evolved. In other cases, total sulfur was determined following combustion and measurement as SO_2 by gas chromatography in a Carlo Erba 1106 Elemental Anayzer. Total (0.18 ± 0.06) and pyrite (0.14 ± 0.05) sulfur were not significantly different (student's 't' test on analyses of 19 slate samples: see app. 3 and 4), as is the case in most marine shales that are low in organic C (Raiswell and Berner, 1986). Iron potentially reactive toward dissolved sulfide was determined by the hot 12N HCl extraction method (Berner, 1970; Raiswell, Canfield, and Berner, 1994) and by dithionite (Canfield, 1989; Raiswell, Canfield, and Berner, 1994); Fe was analyzed by Inductively Coupled Plasma-Atomic Emission Spectroscopy (ICP-AES). Organic carbon was measured on carbonate-free samples (obtained by treatment with 10 percent HCl at room temperature for 24 hrs) followed by combustion and measurement as CO_2 by gas chromatography in a Carlo Erba 1106 Elemental Analyzer. Sulfur isotope analyses were performed on pyrite separated mechanically from the fossil specimens and on CuS precipitates from chromous chloride extractions of adjacent slates and unpyritized fossils. SO_2 gas for isotopic analysis was produced by combustion with Cu_2O (Robinson and Kusakabe 1975), and the purified gas was analyzed on a VG SIRA10 gas source mass spectrometer.

RESULTS

A selection of samples was examined under the SEM (fig. 5). The exoskeleton of the trilobite *Chotecops* shows replacement by a groundmass of euhedral-subhedral cubic crystals of pyrite less than 20 μm in dimension with occasional framboids (fig. 5A, B); larger crystals are scattered through the groundmass (fig. 5A). The texture of the pyrite replacing the skeleton of an asteroid arm is indistinguishable (fig. 5F). The pyrite preserving the appendages of trilobites (fig. 5C, D) and pycnogonids (fig. 5E) occurs as an infill concentrated on the inner surface of the now absent cuticle (hence the outline of the limbs is often apparent in X-radiographs: see fig. 1C). The texture is very similar to that replacing the dorsal exoskeleton of the trilobite, although the proportion of crystals to framboids may vary. The illustrated examples of appendages (fig. 5C-E) show euhedral to subhedral pyritohedra, but examples with cubes also occur perhaps reflecting different levels of local supersaturation (see Murowchick and Barnes, 1987). The structure of the muscle tissue within the limbs is not preserved, in contrast to muscles in phosphatized fossils, where details of the sarcolemma and banding on the fibers, for example, may survive (Martill, 1990; Briggs and others, 1993). Large euhedral cubes of pyrite are occasionally evident on the surface of the Hunsrück Slate fossils (fig. 2B), where they grew presumably at a later stage. The texture of the pyrite in the lens is similar to that in the fossils.

The slates are very uniform in their content of organic C, total and pyrite S, and total Fe (see app. 3 and 4). Concentrations of organic C and pyrite S are both low. Concentrations of organic C in the slates adjacent

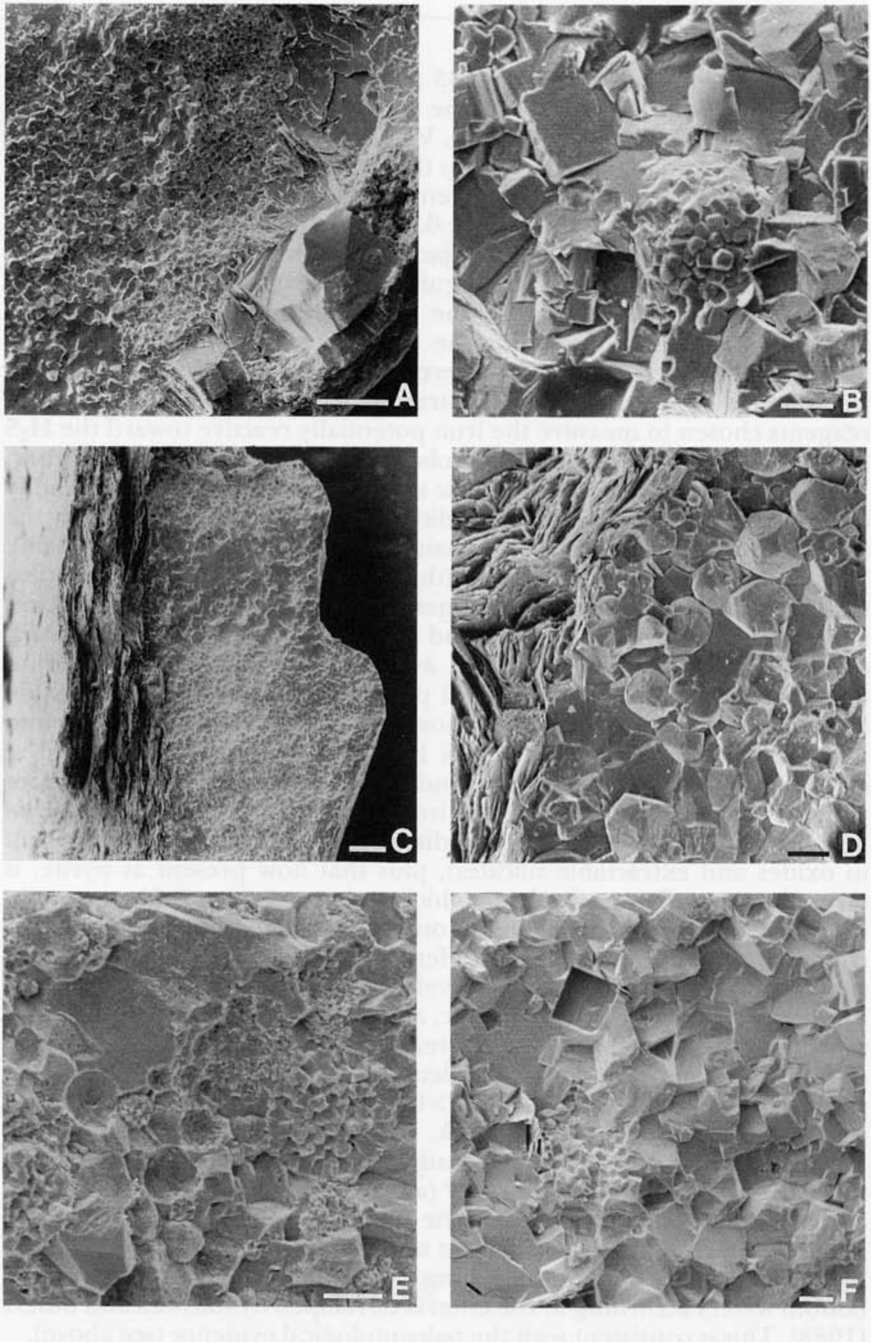

Fig. 5. Scanning electron micrographs of pyrite from specimens from the Eschenberg-Bocksberg Quarry near Bundenbach. A, B. Exoskeleton of the pygidium of the trilobite *Chotecops*. The large crystals in A are near the external surface, but their position within the cuticle varies. Scale bars are 50 μm and 5 μm respectively. C, D. Pyrite infilling of an appendage of *Chotecops*. The clay minerals clearly identify the adjacent matrix. The original cuticle is not preserved. Scale bars are 50 μm and 5 μm respectively. E. Pyrite infilling of an appendage of a pycnogonid. Scale bar is 5 μm. F. Skeleton of an asteroid arm. Scale bar is 5 μm.

to the pyritized fossils averaged 0.33 ± 0.05 wt percent, which is similar to concentrations measured in the block containing the pyrite lens (0.34 ± 0.06 wt percent organic C). Values for pyrite S and total S were also similar in the slates adjacent to the pyritized fossils (0.13 ± 0.05 wt percent and 0.17 ± 0.06 wt percent, respectively) and in the block (0.16 ± 0.20 wt percent and 0.23 ± 0.05 wt percent, respectively).

The total Fe content of slate adjacent to pyritized fossils (5.72 ± 0.29 percent) is larger (and differs significantly at the <1 percent level: student's 't' test) than that in the slates around unpyritized fossils (5.21 ± 0.37 percent) (including the 10 supplementary specimens: app. 2) and in the block (5.44 ± 0.20 percent). There are also differences in the amount of Fe that can be extracted from these samples by acid reagents chosen to measure the iron potentially reactive toward the H_2S produced by sulfate reducing microbes (Raiswell, Canfield, and Berner, 1994). Buffered dithionite is specific to the iron oxides that react readily to form pyrite; boiling 12N HCl additionally extracts some iron from the slowly reacting iron-silicate pool (Raiswell, Canfield, and Berner, 1994). The total Fe in the iron oxide pool (that is, the amount within pyrite plus that extracted by dithionite) averages 0.26 ± 0.08 percent in the slates adjacent to the pyritized fossils and 0.14 ± 0.03 percent in the block containing the pyrite lens. These averages are significantly different (student's 't' test) only at about the 1 percent level. However, some oxide iron remaining after pyrite formation may have been incorporated into metamorphic chlorite. Boiling 12N HCl extracts approx 40 percent of chloritic iron (Raiswell, Canfield, and Berner, 1994) and may therefore provide a better estimate of the iron potentially available for pyrite formation in these slates. The iron dissolved in HCl (that is, that present in oxides and extractable silicates), plus that now present as pyrite, is termed potentially reactive iron, which averages 2.66 ± 0.91 percent in the slates adjacent to the fossils but only 1.14 ± 0.35 percent in the block containing the pyrite lens. This difference in potentially reactive iron is significant at the <0.01 percent level. Host slates in the block are fairly uniform with respect to total, pyritic, and dithionite Fe contents but show a pronounced peak in potentially reactive iron across the lens horizon (fig. 6A). Immediately above the lens horizon the ratio of potentially reactive iron/total Fe in the slate is >0.25, compared to about 0.15 at the upper and lower edges of the block. By contrast the ratio of potentially reactive iron/total Fe in the slates adjacent to pyritized fossils is usually more than 0.3 and ranges up to 0.7 (avg 0.44 ± 0.16). Values for degree of pyritization (DOP: Pyrite Fe/Pyrite Fe + HCl soluble Fe) show a range of 0.02 to 0.20 in the slates adjacent to the fossils and 0.08 to 0.32 in the block (see app. 3 and 4), indicating deposition from fully-oxygenated bottom waters according to the criteria developed by Raiswell and others (1988). This is consistent with the paleontological evidence (see above).

The $\partial^{34}S_{CDT}$ of pyrite sulfur in the block containing the pyrite lens shows marked fluctuations, ranging from −24.7 to +34.4 permil (fig. 6B; see app. 3). In the slates above the lens, $\partial^{34}S_{CDT}$ varies between −24.7 and

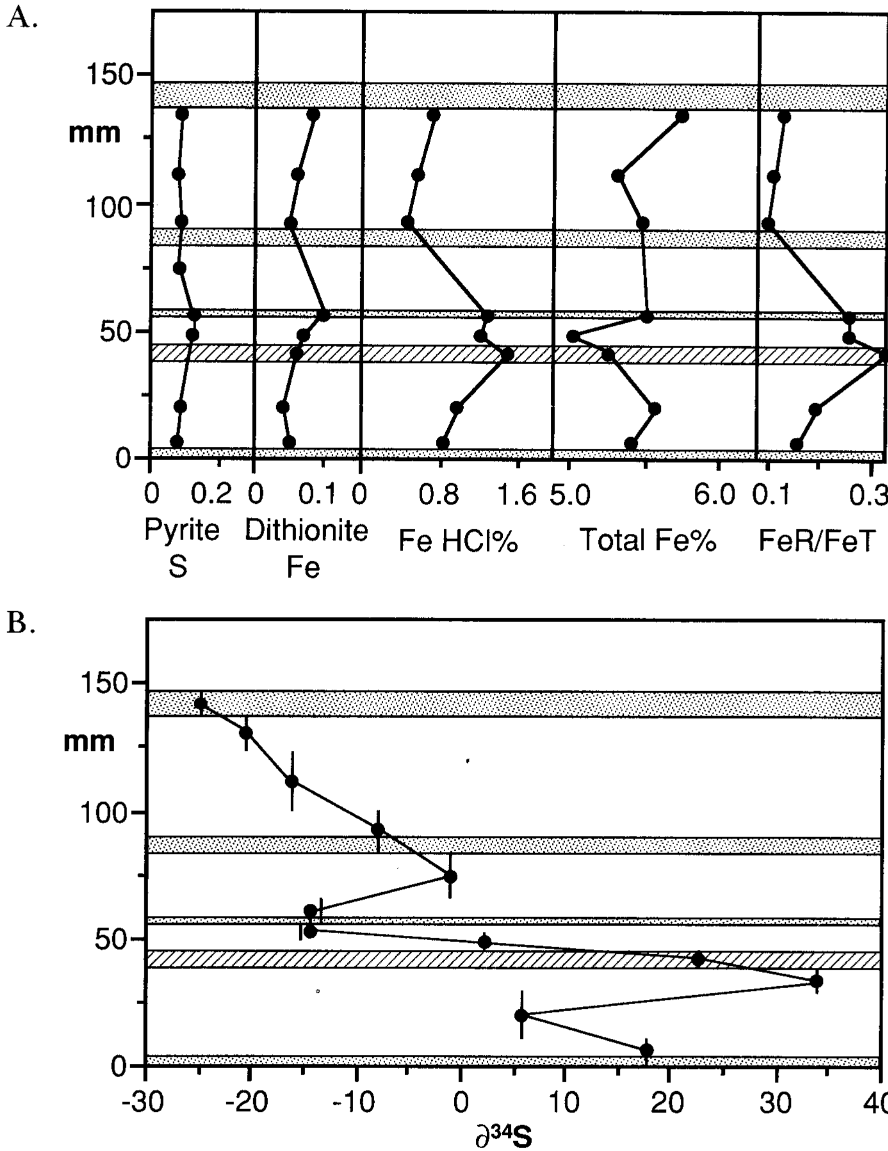

Fig. 6. A. Chemical and B. isotopic gradients through a 15 cm block of slate (from the Eschenbach-Bocksberg Quarry) which hosts a pyrite lens. The cross-hatched area represents the level of the lens; the stippled areas represent lighter colored slightly coarser mudstone which forms the base of individual microturbidites. The vertical extent of the bars represents the thickness of sample analyzed. The values at the level of the lens represent the host slate rather than the lens itself.

0 permil, whereas in the vicinity of the lens pyrite $\partial^{34}S_{CDT}$ shows a marked excursion to more positive values reaching +22.5 permil in the slates at the level of the lens and up to +34.4 permil in the 1 cm below it. Below this excursion, pyrite $\partial^{34}S_{CDT}$ falls (+6 to +18 permil), but the values are still higher than those in the slate above the lens. The lens itself gives values of +6.8 to +7.5 permil. Thus the sulfur isotope composition of the lens is lighter than the adjacent slate. The excursion in the vicinity of the lens (fig. 6B) clearly indicates that some exceptional process of pyritization was involved in its formation.

The slates associated with fossils, in contrast to those in the vicinity of the lens, are ^{34}S depleted (see app. 1). The range of $\partial^{34}S$ found within the unpyritized fossils (−15.5 to +0.2 permil) lies within that for pyrite in the adjacent slate (−19.2 to +12.3 permil) and for pyrite in slate adjacent to pyritized fossils (−28.3 to +10.4 permil). The means and standard deviations of these samples overlap, and a student's 't' test reveals no significant differences (unpyritized fossils -6.3 ± 7.1 permil, slates adjacent to them -7.9 ± 9.5 permil, and slates adjacent to pyritized fossils -12.0 ± 11.6 permil). However, all three sets of samples are significantly different (at the <1 percent level) from the $\partial^{34}S$ values of pyritized fossils, which range from −4.9 to +26.9 permil, with an average of $+8.0 \pm 9.3$ permil.

The slate surrounding pyritized fossils is depleted in ^{34}S relative to the fossils themselves, and the gradient is sharpest over the 2 cm interval adjacent to the specimen (fig. 7; app. 1). In only one case, a crinoid calyx (no. 4, fig. 7, app. 1), is a pyritized fossil similar in $\partial^{34}S_{CDT}$ to the surrounding slate. By contrast the value obtained from samples including unpyritized fossils is isotopically much closer to the surrounding slate. The pyrite within different fossil taxa and within different parts of individual fossils (but only three specimens were sub-sampled) yields small but consistent differences in sulfur isotope composition (see app. 1). Pyrite associated with organic tissues (limbs of the pycnogonid *Palaeoisopus* and trilobites) is lighter (^{34}S-depleted) than pyrite associated with biomineralized tissues (trilobite exoskeleton, echinoderm ossicles). The more ^{34}S depleted isotopic composition correlates with the presence of larger quantities of readily metabolized tissue.

INTERPRETATION

The critical observations concern: (1) the relative abundances of the different forms of iron in the block containing the lens and in the slates adjacent to fossils (both pyritized and unpyritized), (2) the concentrations of organic matter in the sediments, and (3) the isotopic differences within the block and between pyrite in fossils and in the adjacent slate.

Abundance and Form of Sediment Iron

Our earlier study of Beecher's Trilobite Bed (Briggs, Bottrell, and Raiswell, 1991) indicated that a high concentration of iron in the sediment might be one factor crucial in facilitating the pyritization of readily

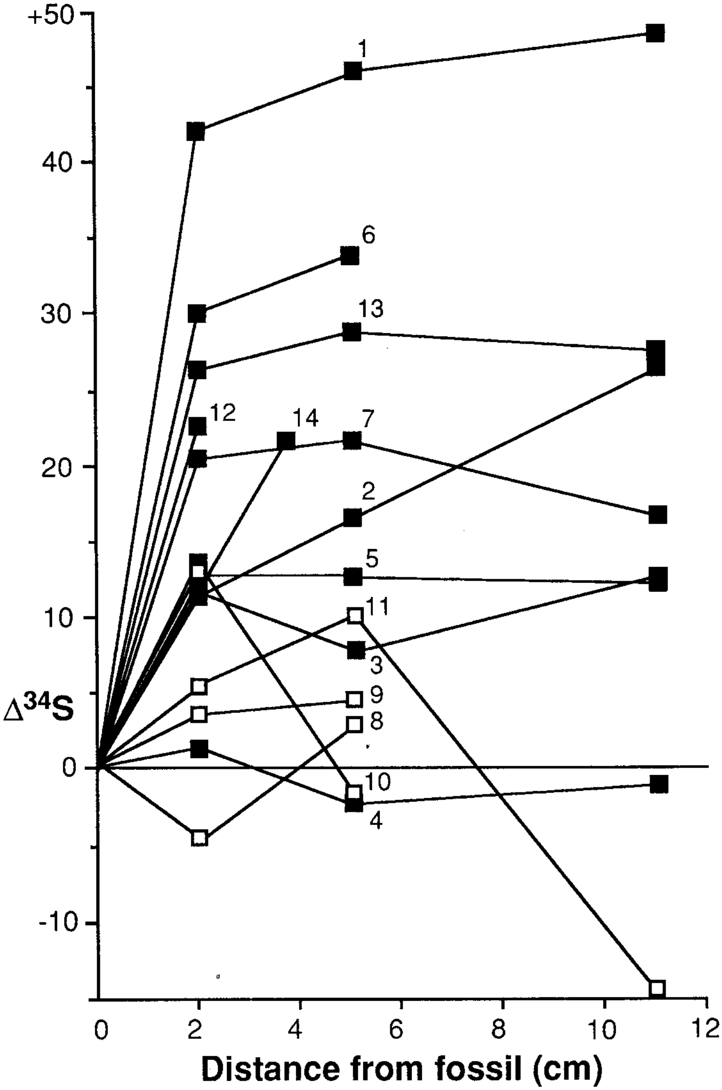

Fig. 7. Gradients in sulfur isotopic composition with distance from a fossil in the same bed (for data and identity of fossils see app. 1). The difference in sulfur isotope composition ($\Delta^{34}S = \partial^{34}S_{fossil} - \partial^{34}S_{sediment}$) is plotted against distance from the fossil (where more than one analysis was performed on a fossil a mean value for $\partial^{34}S_{fossil}$ is taken). For the pyritized fossils (solid squares) $\Delta^{34}S$ increases sharply in the sediment, the only exception being the crinoid calyx (4). The behavior of the unpyritized fossils (open squares) is variable, but increases in the sediment are much smaller (9) or are reversed in the outermost samples (8, 10 and 11).

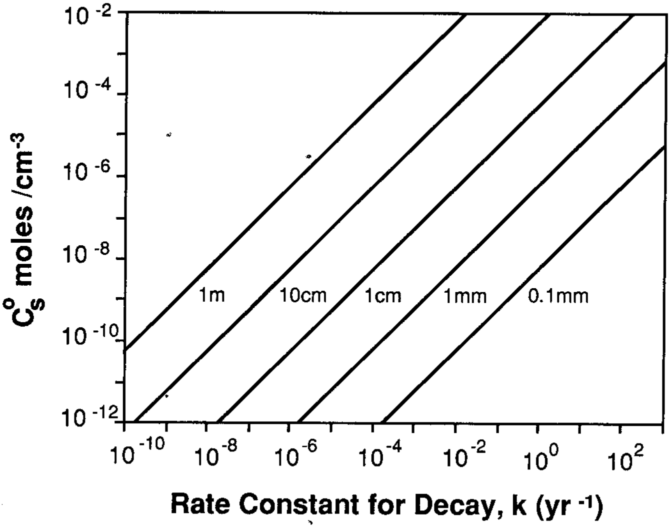

Fig. 8. The relationship between C_S°,(concentration of dissolved sulfide) and R (rate constant for sulfate reduction) plotted for a = 0.1 mm, 1.0 mm, 1 cm, 10 cm and 1 m.

metabolizable soft tissue. Data from the Russian and North American platforms (Ronov and Migdisov, 1971) suggest that the total iron content of Paleozoic shales is reasonably uniform at 3.9 to 4.3 percent (table 1). By comparison the Devonian Hunsrück samples are all rich in total Fe, but concentrations around pyritized fossils (5.72 ± 0.29 percent) are higher than those in the block (5.44 ± 0.20 percent), which in turn exceed those in unpyritized fossils (5.21 ± 0.37 percent).

The high total iron contents of the Hunsrück Slates and the differences between the slates around pyritized and unpyritized fossils are unlikely to have arisen through metamorphism for the following reasons: (1) Metamorphism to grades higher than in the Hunsrück Slates (that is, above the anchizone) is generally required to mobilize iron by transforming pyrite typically to pyrrhotite (Hall, Boyce, and Fallick, 1987) which does not occur in the Hunsrück Slates. (2) Even if iron and sulfur were mobilized they would normally be reprecipitated locally into sulfide blebs or porphyroblasts and associated chlorite or chloritoid (Hall, Boyce, and Fallick, 1994) without reducing the total iron content. By contrast the Hunsrück pyrite is fine-grained and disseminated in the slates surrounding the fossils, and there is no textural evidence of mobilization (fig. 5).

A similar conclusion emerges from a comparison of total Fe data from the Hunsrück Slate with those from shales deposited beneath an oxygenated water column (that is, the environment of the Hunsrück Slates) through geological time (Raiswell and Al-Biatty, 1989, 1992). These data (table 1) were obtained from samples originally collected by

TABLE 1

A compilation of total iron data from the era-averages of Ronov and Migdisov (1971) covering the Proterozoic, Paleozoic and Mesozoic plus Cenozoic. Additional data collected by Raiswell and Al-Biatty (1989, 1992) utilizing a selection of the Raiswell and Berner (1986) normal marine samples of Cambrian to Jurassic age to derive total Fe contents and the ratio Potentially reactive Fe/Total Fe

Normal marine (Raiswell and Al-Biatty, 1989, 1992)				Era averages (Ronov and Migdisov, 1971): Russia Platform	Era averages (Ronov and Migdisov, 1971): North American Platform
Cretaceous		—	Mesozoic + Cenozoic	4.08	2.03
Jurassic		4.10			
Triassic		—			
Carboniferous		2.51	Paleozoic	4.31	3.90
Devonian		3.46			
Silurian		—			
Ordovician	Upper	3.91			
	Lower	4.11, 4.69, 4.91			
Cambrian	Upper	7.29			
	Middle	1.80			
			Late Proterozoic	5.45	—

Normal marine data from Middle Cambrian, Georgina Basin, Australia (9 samples); Upper Cambrian, Outwoods Shales, UK (23); Lower Ordovician Deanshanger (17), Lillingstone Lovell (19) and Great Paxton (23), UK; Upper Ordovician Oslo, Norway (11); Lower Carboniferous, Bowland Basin, UK (10); Upper Devonian, New Albany Formation, USA (9); Lower Jurassic, Robin Hoods Bay, UK (26). Era averages are composites of 34 samples from 1226 specimens (Late Proterozoic), 401 samples from 6734 specimens (Paleozoic, Russian Platform), 473 specimens (Paleozoic, North American platform), 259 samples from 2764 specimens (Mesozoic plus Cenozoic, Russian Platform), 959 specimens (Mesozoic plus Cenozoic, North American Platform).

Raiswell and Berner (1986) to study organic C and pyrite sulfur variations. The data set is neither large (147 samples) nor comprehensive (mainly Cambro-Ordovician in age), but, with one exception, the total Fe values are 1 to 3 wt percent lower than observed in the samples with pyritized fossils from the Hunsrück Slates. These differences in wt percent Fe cannot be attributed simply to metamorphic loss of CO_2 (a loss of 10 wt percent of the Hunsrück Slate would have been required to increase the proportion of Fe by even 0.5 percent).

These data sets suggest that the slates surrounding the Hunsrück Slate fossils are enriched in total Fe compared to typical Paleozoic marine shales. The range of potentially reactive iron/total Fe in the Hunsrück Slates surrounding the pyritized fossils (0.19-0.70, mean 0.46 ± 0.16) overlaps that in ancient normal marine settings (table 1: values range from 0.43-0.90, weighted mean of 0.57 ± 0.14) with lower values of 0.10

to 0.33 in the block (fig. 6A). Thus the ratios of potentially reactive iron/total iron in the Hunsrück Slates are comparable to those in other normal marine shales, and the high total Fe values may indicate a potential to sustain high concentrations of dissolved Fe during shallow burial pyritization. While concentrations of HCl-soluble Fe are high in the Hunsrück Slate, dithionite-soluble Fe concentrations are low (app. 4). An important issue therefore is how readily iron could be solubilized from HCl-soluble phases. Because of their reactivity, labile oxide phases are unlikely to survive diagenesis and metamorphism. Thus the present low concentrations of dithionite Fe in the Hunsrück Slates do not indicate that the *depositional* concentrations of iron oxides were low. Modern normal marine sediments appear to show that both dithionite and HCl-soluble Fe increase with increasing total iron content (Raiswell, unpublished data). Therefore, the high concentrations of reactive and total Fe in the Hunsrück Slate suggest that high concentrations of oxides were also available at deposition. Such oxides could sustain high concentrations of porewater dissolved iron in the absence of appreciable H_2S production by sulfate reduction. Suppression of sulfate reduction occurs when sediments contain low concentrations of metabolisable organic matter (Aller, Mackin, and Cox, 1986; Canfield, 1989). Although the present organic C contents of the Hunsrück Slates are certainly low (0.3-0.4 percent C), thermal and burial effects will have caused a considerable loss of carbon (see below).

The iron data provide a clue to the likely mechanisms and controls on pyritization in the Hunsrück Slates. The analyses of the block show that there are stratigraphic variations in the proportions of potentially reactive iron/total iron (fig. 6A; app. 3). It is uncertain whether the increase in this ratio above the pyrite lens was the result of a migration of iron from the adjacent sediment into the lens during its formation or whether it reflects original compositional variations. However, the relatively low values for the ratio of potentially reactive iron/total iron in the block compared to those in other Hunsrück Slate samples (app. 4) suggest that diffusional migration of iron from the sediments into the lens was the more likely possibility.

Concentrations of organic matter.—Concentrations of organic matter in the slates are uniformly low around the pyritized and unpyritized fossils and in the block (0.36 ± 0.08 percent C). However, these concentrations reflect the effects of continued burial, thermal, and diagenetic processes. In normal marine sediments (like the Hunsrück Slates) about 75 percent of carbon is consumed by processes following sulfate reduction up to and including greenschist facies metamorphism (Raiswell and Berner, 1987). The neogenesis of chlorite and mica, as well as the growth of chlorite muscovite porphyroblasts (Talbot, 1964; Roy, 1978), indicates that metamorphism attained upper anchizone or lowest greenschist facies conditions in the Hunsrück Slate. Thus the original carbon content is likely to have been 1 to 1.5 percent. Some of the most metabolizable organic carbon might have been broken down by decay before burial. Thus there was only a comparatively small content of carbon available for sulfate reduction in the original sediment, and this is reflected in the low concentrations of pyrite. The formation of pyrite was not iron-limited; the slates still contain iron capable of reacting with H_2S, and DOP values are low. Moreover porewater sulfate was not completely depleted by sulfate reduction; the $\partial^{34}S_{CDT}$ value of pyrite in the slate (see below), particularly in the vicinity of the fossils, is smaller than that of Devonian seawater sulfate (+17 permil; Claypool and others, 1980).

Sulfidization processes in modern sediments low in organic carbon but with significant concentrations of reactive iron are iron-dominated, that is, dominated by Fe reduction. Intensive reworking of the sediments of the Amazon inner shelf (Aller, Mackin, and Cox, 1986), for example, promotes the degradation of all but poorly metabolizable organic matter and introduces O_2, maintaining suboxic conditions in the porewaters. Sulfate reduction is suppressed, and iron reduction results in porewaters that are unusually rich in dissolved iron (up to 1 mM). Some iron is precipitated as siderite, but more is laterally exported during reworking. Reworking also promotes the recharge of iron oxides through the oxidation of dissolved and sulfidic iron. The turbiditic nature of the Hunsrück sediments may have similarly favored suboxic diagenesis. Estimated concentrations of organic C in the Hunsrück Slates (1-1.5 percent) are higher than those in the Amazon inner shelf sediments (0.45-0.77 percent C). However, the ratio of Fe/C (0.18-0.26 for original C contents of 1-1.5 percent) places the Hunsrück Slates with the sediments of the Amazon inner shelf (0.12) and Mississippi Delta (0.20) with higher Fe and lower C than typical marine sediments (Aller, Mackin, and Cox, 1986).

Sulfur isotope composition.—The $\partial^{34}S_{CDT}$ of Lower Devonian seawater sulfate was ~17 permil (Claypool and others, 1980). During microbial sulfate reduction, ^{32}S is more rapidly reduced than ^{34}S (Kaplan and Rittenberg, 1964; Chambers and Trudinger, 1979; Nakai and Jensen, 1967). Therefore, dissolved sulfide enriched in the lighter isotope relative to seawater sulfate is incorporated into pyrite, until the pore system becomes closed to the renewal of sulfate from the overlying seawater, following which the proportion of ^{34}S in pore fluids progressively increases. Given a $\partial^{34}S$ value for seawater of ~17 permil, typical maximum fractionations of −45 to −60 permil (Goldhaber and Kaplan, 1974) would give pyrite formed from an unlimited marine reservoir a $\partial^{34}S$ value of −28 to −43 permil. However, the $\partial^{34}S$ of pyrite in most of the samples analyzed in the present study is substantially larger than −28 permil. Complete reduction of sulfate in a closed system where no H_2S is lost would give a bulk pyrite with a $\partial^{34}S_{CDT}$ value the same as that of the original seawater sulfate (+17 permil). Except in the vicinity of the lens the Hunsrück Slate samples range from −28 to +17 permil which indicates varying degrees of open system (producing ^{34}S depleted pyrite) versus closed system (producing isotopically heavy pyrite) behavior or loss of H_2S from the sediment. Equally a single system could evolve from open to closed conditions, with +17 permil representing the presence of a late phase of FeS_2 formation or the addition of isotopically heavy sulfur to an isotopically light precursor FeS phase. The thickness of sediment introduced by turbiditic sedimentation may have inhibited the diffusion of sulfate from overlying seawater to the position of a decaying carcass, thus creating a closed system (and ^{34}S enriched pyrite) at relatively shallow burial depths.

$\partial^{34}S$ values larger than those of the original seawater are uncommon among the Hunsrück fossils and their associated slates, occurring only in some crinoid stems and in the block. The block shows a fluctuating profile with an overall increasing ^{34}S enrichment toward its base, with the most extreme value (+34 permil) recorded just below the level of the pyritic lens. The $\partial^{34}S$ values in this region exceed those that could occur from complete reduction of Devonian seawater in a closed system. Thus some exceptional process, which did not affect the fossils with pyritized soft-tissues, must have operated. Complete reduction of sulfate in a clastic sediment with a porosity of about 85 percent produces about 0.2 wt percent pyrite sulfur (Berner 1964a). Because the Hunsrück Slate samples average only 0.09 percent pyrite sulfur, it is likely that there was residual sulfate in the pore water once sulfate reduction was completed. Additional sulfate may have been consumed to produce H_2S that was lost from the sediment by diffusion, but such loss is unlikely to have been significant in the presence of abundant iron reactive to H_2S that would have trapped it. Thus residual sulfate, which was isotopically heavier than +17 permil (due to the preferential removal of $^{32}SO_4$), could diffuse to isolated sites where sulfate reduction continued. The lens in the block was clearly such a site.

Sulfate would have to diffuse from a substantial volume of sediment to yield the concentrations of isotopically heavy pyrite observed in the vicinity of the lens. The very enriched $\partial^{34}S$ value (+34 permil) for the 0.7 percent pyrite sulfur in the sample immediately below it suggests that residual ^{34}S-enriched sulfate was transported from the sediments beneath. Although the signal is most pronounced below the lens, a high value (+22.5 permil) also occurs in the slate at the level of the lens. The lens itself, however, yields lower $\partial^{34}S_{CDT}$ values (+6 to +8 permil). This is a reflection of its large mass (it is about 6 cm in maximum dimension parallel to bedding) which incorporates a much higher proportion of lighter early formed pyrite, resulting in a lower average value than that in the immediately adjacent sediment. The chemical and isotopic trends within the block preserve evidence of the transport of Fe and sulfate to a region of locally-enhanced sulfate reduction at the lens site. The lens produced significant perturbations in the chemistry of the adjacent sediment because the mass of material required for its formation was large.

Similar processes to those affecting the lens occurred in association with the fossils, but the smaller quantities of S and Fe involved in their pyritization were sourced from the adjacent sediment. Pyritized fossils are almost always enriched in ^{34}S relative to their surrounding slate, and the gradient is sharpest over the 2 cm interval immediately around the fossil (fig. 7). By contrast the slate immediately enclosing unpyritized fossils is isotopically similar to that in the samples taken at 1 to 3 and 4 to 6 cm distance. These observations suggest that later (but still precompactional) ^{34}S enriched pyrite was formed in a closed system immediate to the pyritized fossils. The H_2S formed at this stage did not diffuse out into the surrounding sediment, and its efficient trapping can be attributed to the high reactive iron content of the surrounding sediment, which allowed rapid pyritization of soft tissue to occur. There is, however, considerable variation in the degree of soft-tissue pyritization (Kott and Wuttke, 1987; Bartels and Brassel, 1990). The unpyritized trilobites from the Eschenbach-Bocksberg quarry (app. 1, 4, samples 8, 10, 11) are articulated specimens, demonstrating that they too were carcasses rather than moults and had undergone rapid burial. Given that similar conditions appear to have prevailed, the lack of pyritization of these specimens presumably reflects rapid degradation of the most readily metabolized tissue prior to or immediately following burial. This cannot be attributed to any taxonomic difference and presumably reflects lower sedimentation rates and shallower burial. An alternative explanation may apply in the case of the unpyritized fossils from elsewhere (app. 1, 4, sample 9; app. 2) where the associated slate is relatively low in total Fe (5.02 ± 0.32 percent), as are ratios of potentially reactive Fe/total Fe (0.33 ± 0.08). These data suggest that the low iron content may have inhibited early pyritization.

COMPARISON WITH BEECHER'S TRILOBITE BED

During the Ordovician when Beecher's Trilobite bed was deposited, seawater sulfate had a $\partial^{34}S$ value comparable to that in the Lower Devonian (about +17 permil, Claypool and others, 1980). Hence the $\partial^{34}S$ values of the Beecher's Bed and Hunsrück Slate faunas can be directly compared assuming that the processes operating were the same. The range of $\partial^{34}S_{CDT}$ values obtained for the trilobites in Beecher's Trilobite Bed (Briggs, Bottrell, and Raiswell, 1991) (−3 to +21 permil for the exoskeleton and +10 to +27 permil for the limbs) is similar to that obtained for the fossils in the Hunsrück Slate (see app. 1). However, the limbs of the Beecher's Bed trilobites show values consistently larger than those of the exoskeletons (Briggs, Bottrell, and Raiswell, 1991, fig. 3) whereas in the trilobites of the Hunsrück Slate (see app. 1) the values for limbs are slightly smaller. This may reflect more prolonged pyrite formation in the limbs of the Beecher's Bed trilobites, where long crystals radiate from a nucleus of fine-grained aggregates resulting in "floriform" structures 11 to 15 μm in diameter (Briggs and Edgecombe, 1993, fig. 5), in contrast to the granular pyrite and simple framboids 11 to 12 μm in diameter that occur in the Hunsrück Slate fossils (fig. 5).

Values for $\partial^{34}S_{CDT}$ in the slates adjacent to the Hunsrück Slate fossils do not reach the isotopic compositions in excess of +30 permil that characterize the layer containing the Beecher's Bed trilobites (Briggs, Bottrell, and Raiswell, 1991). Such a value is reached, however, immediately below the pyrite lens in the block of Hunsrück Slate where $\partial^{34}S_{CDT}$ is +34.4 permil. Sediment pyrite must have continued to form here for longer than it did in association with the pyritized fossils. These extreme $\partial^{34}S$ values may reflect the potential of larger masses of organic matter (as represented by the lens and the concentration of trilobites within the single horizon of Beecher's Bed) to deplete their surroundings of sulfate, in contrast to the smaller scattered fossils in the Hunsrück Slates. The lighter values in the lens itself reflect some unknown mixture of light and heavy isotope values.

Analyses of total Fe for 20 Beecher's Bed samples from 20 cm of section that includes the 4 cm Beecher's Trilobite Bed yield values ranging from 4.74 to 6.05 percent (mean 5.31 ± 0.44 percent) with 5.55 percent in the bed itself. These, like the values for the Hunsrück Slate, are relatively high for normal marine sediments (table 1), suggesting that Fe concentrations were a control on pyritization. The lack of pyritized trilobites in the layers above and below the Trilobite Bed is consistent with the absence of any evidence for complete carcasses trapped by rapid burial.

A MODEL FOR SOFT-TISSUE PYRITIZATION

We argue above that the Hunsrück Slates were iron rich and depleted in readily metabolizable organic C, resulting in the suppression of sulfate reduction and the maintenance of high concentrations of dissolved iron in porewaters during diagenesis. However, this environment is in sharp contrast to that around a decaying carcass, which produces a microenvironment rich in readily metabolizable organic matter but with little sediment to source iron. In this anaerobic microenvironment sulfate reduction proceeds

$$2CH_2O + SO_4^{2-} \rightarrow H_2S + 2HCO^{3-}$$

using sulfate derived from the surrounding porewaters and overlying seawater (Berner, 1970; Goldhaber and Kaplan, 1974; Berner, 1984). The microbially produced H_2S then reacts with dissolved Fe from the surroundings to form either iron monosulfides (which are later transformed to pyrite) or pyrite directly (Berner, 1970; Rickard, 1975; Howarth, 1979; Schoonen and Barnes, 1991a, b; Rickard, Schoonen, and Luther, 1995).

The high degree of replication during pyritization (pseudomorphous replacement) is a product of the high reactive Fe and low content of metabolizable C in the host sediments, which maintain relatively high concentrations of dissolved iron and sulfate in the porewaters. As a consequence of these conditions the requisite gradients can develop, with diffusion of sulfate and iron toward the fossils allowing continued sulfate reduction and pyrite formation. Most importantly sulfide is unable to diffuse appreciably beyond the carcass, and the efficient trapping of H_2S allows rapid pyritization of the soft tissue.

The localized occurrences of pyrite within fossils can be explained by the interaction of two variables: the concentration of dissolved sulfide at the decay site and the concentration of dissolved iron in the surrounding porewaters (Canfield and Raiswell, 1991; Raiswell and others, 1993). The situation can be modelled by envisaging a spherical reservoir which contains dissolved sulfide (representing bacterial sulfate reduction of soft tissue at the fossil site) which is immersed in dissolved ferrous iron (generated via iron reduction and representing porewaters in the surrounding sediments). Solutes are free to diffuse, react, and precipitate within and between the reservoirs, and the locus of precipitation is controlled by the activity products and the dictates of thermodynamics and kinetics. Raiswell and others (1993) derived a three-dimensional model assuming a spherical site of organic matter decay completely buried in a sediment with iron-rich porewater. The model is quantified by an expression that determines the location of maximum precipitation (R_{jmax}) at the steady state

$$R_{jmax} = \frac{a(D_S C_S^\circ + D_F C_F^\circ)}{D_F C_F^\circ} \tag{1}$$

where a is the radius of the organic matter sphere, D_S, D_F are the diffusion coefficients for dissolved sulfide and iron, respectively, C_S° is the steady state concentration of dissolved sulfide generated by sulfate reduction at the site of organic matter decay, and C_F° is the steady state concentration of dissolved iron in the surrounding pore waters (which is assumed to remain constant at a specified value).

Eq 1 can be simplified, using values of $D_S = 376\ \text{cm}^2\ \text{yr}^{-1}$ and $D_F = 149\ \text{cm}^2\ \text{yr}^{-1}$ (from Boudreau and Canfield, 1988), to

$$R_{jmax} = a\left(\frac{2.52 C_S^\circ}{C_F^\circ} + 1\right) \tag{2}$$

Although the model does not allow precipitation to occur at the decay site (the region between 0 and a), the probable circumstances in which this would occur can be predicted using eq. 2. Clearly R_{jmax} approaches a for $C_S^\circ/C_F^\circ \ll 1$; that is, iron-rich pore waters are required to confine precipitation to the decay site. Where high C_S°/C_F° values prevail at the decay site, dissolved sulfide would tend to migrate away from the organism creating a precipitation front through the surrounding sediments (Coleman and Raiswell, 1995). Here an arbitrary value of $C_S^\circ/C_F^\circ < 0.1$ is chosen to confine pyritization to the vicinity of the decaying organism (to make R_{jmax} approach a). The isotope data (app. 3) confirm that there was little sulfide escape from decaying organisms that were pyritized in the Hunsrück Slate. The ^{34}S-enriched sulfide found in the fossil is absent from the surrounding slates, although DOP values indicate that iron was available to react with any sulfide diffusing away from the fossil.

Raiswell and others (1993) derived an expression for the steady state concentration of dissolved sulfide ($C_S°$) maintained by the decay of the organic matter sphere (radius a)

$$C_S° = 1.6 \times 10^{-5} a^2k \text{ moles cm}^{-3} \tag{3}$$

where k is the first-order rate constant for sulfate reduction at the sphere. This relationship between $C_S°$ and k is plotted in figure 8 for values of radius a from 100 μm to 1 m.

Rate constants calculated from modern sediments typically range from 10^{-1} to 10^{-6} yr^{-1} (Middelburg, 1989). These sediment values are probably representative of mixed organic matter (marine and terrestrial) which has partially decayed in the water column and at the sediment-water interface. Experimental values of about 1–10 yr^{-1} for fresh planktonic material (Westrich and Berner, 1984) are likely to be a better approximation for soft tissue.

Small masses of organic matter (r = 1 mm to 1 cm) with k values of 1–10 yr^{-1} can sustain concentrations of dissolved sulfide of 10^{-6} to 10^{-3} moles cm^{-3} (10^{-3} 1 molar) (fig. 8). Porewater concentrations of dissolved iron at least one order of magnitude higher than this ($C_S°/C_F° < 0.1$) would be necessary to confine pyrite formation to the decay site. In the near-surface layers of modern sediments, however, porewater iron concentrations are commonly only in the range of 10^{-4} to 10^{-5} molar (or 10^{-7} to 10^{-8} mol cm^{-3}), because the dissolved Fe is titrated by dissolved HS^- (Canfield and Raiswell, 1991). Higher iron concentrations (up to 7×10^{-4} molar) are found where the production of dissolved sulfide is suppressed (Aller, Mackin, and Cox, 1986). Thus, although undoubtedly oversimplified, the model confirms that unusually high concentrations of porewater iron are necessary for soft-tissues to be pyritized selectively.

Previously Brett and Baird (1986) emphasized the role of metabolizable organic matter in the formation of pyrite and suggested that burial of local concentrations of organic matter in otherwise organic-poor sediments is important in the pyritization of soft-parts. However, it is evident that it is the *distribution* of metabolizable organic matter (that is, local enrichments in sediment otherwise poor in labile carbon) that is critical. Allison (1988) recognized that selective (pseudomorphous) soft-tissue pyritization is favored by a low organic content and rapid sedimentation (in marine clastics where the oxic/anoxic boundary is at or just below the sediment-water interface). Such conditions are relatively widespread, however, and it is now clear that an additional factor, unusually high levels of reactive iron, is required.

CONCLUSIONS

The isotope and chemical data demonstrate that diagenetic conditions in the Hunsrück Slate, like those in Beecher's Bed (Briggs, Bottrell, and Raiswell, 1991) were unusual, and this explains why soft tissue pyritization is so rare.

1. The slates surrounding the fossils are low in organic C and pyrite S. The amounts of pyrite S are generally lower than would be expected

for reduction of seawater sulfate in a closed system at the typical porosities of fine-grained sediments. This indicates low-level sulfate reduction in the adjacent sediments. Pyrite in the slates is generally ^{32}S-depleted, however, and *never* reaches the isotopic composition of Lower Devonian seawater (+17 permil). Thus residual sulfate must have been present when pyrite formation ceased. Pyrite formation in the sediments was not, therefore, sulfate limited.

2. The slates surrounding the fossils now contain high concentrations of HCl-soluble Fe, which may have been reactive toward dissolved sulfide during diagenesis. DOP values range from 0.04 to 0.20, indicating that pyrite formation was not iron-limited. However, pyrite formation in the sediments could have been limited by the low concentrations of metabolizable organic matter which were sufficient to sustain iron reduction (but not sulfate reduction), thus making Fe and sulfate available to sustain sulfide formation at the soft tissue decay site.

3. The slates surrounding the Hunsrück fossils are unusually rich in total Fe compared to marine shales from elsewhere (table 1). However the proportion of this total Fe that is potentially reactive toward dissolved sulfide is similar to that in other Paleozoic normal marine shales. Thus the higher total Fe content could have produced porewaters unusually rich in dissolved iron during shallow burial, provided concentrations of organic matter were sufficient to support only iron reduction and not sulfate reduction.

4. The readily metabolizable soft tissue in a Hunsrück carcass would promote sulfate reduction, creating local microenvironments rich in dissolved sulfide. The surrounding sediments supplied sulfate and iron that sustained pyrite formation at the decay site. The sulfur isotope compositions of the pyritized fossils are significantly ^{34}S-enriched relative to the pyrite in the surrounding slates indicating that pyrite formation continued at the decay site until the surrounding porewaters became sulfate-depleted. There is no evidence for the diffusion of ^{34}S-enriched sulfide away from fossils into the surrounding sediments. Thus, sulfide was trapped by porewaters rich in dissolved Fe, allowing pyritization of the carcass to occur quickly and efficiently.

5. Pyritized fossils are rare in the Hunsrück Slate, and usually represent isolated sites of metabolizable carbon. In the Ordovician Beecher's Bed, the pyritized fossils are concentrated in a 4 cm thick layer providing a metabolizable fill in an otherwise C-poor sandwich. In both cases, soft tissues are preserved as an infill or coating of pyrite that varies in its completeness. The texture combines framboids and cubes or pyritohedra less than 20 μm in size with occasional larger euhedral crystals (fig. 5). The structure of the soft-tissues (for example, muscle fibers) is not preserved. Biomineralized skeletons show a veneer of pyrite on the surface, pyrite precipitation within voids, or replacement of the original mineral.

6. A combination of two factors is crucial to soft-tissue pyritization, rapid burial, and sediment chemistry. Carcasses must be buried rapidly to avoid breakdown by benthic scavengers under oxic conditions. The

surrounding sediment must contain (1) low concentrations of available organic matter (hence pyrite formation is organic matter-limited, and residual dissolved iron and sulfate can migrate to the decay site) and (2) unusually high concentrations of iron that is reactive toward dissolved sulfide, permitting rapid and efficient pyritization of the soft tissue.

ACKNOWLEDGMENTS

The research was supported by the Natural Environment Research Council (GR9/518; stable isotope facilities provided by GR3/6254). We are grateful to the owners of Schiefergrübe Eschenbach-Bocksberg, Johann and Backes, for access and for assistance in obtaining samples. Owen Sutcliffe kindly drafted figures 3 and 4. We thank P. A. Allison, C. J. Underwood (who took the SEM photographs in fig. 5), and R. J. Parkes for helpful discussions, and Carl Brett, Howard Feldman, Michelle Tuttle, and two anonymous referees for constructive criticism of earlier versions.

Appendix 1

Fossils and associated matrix sediments: Isotopic data ($\partial^{34}S_{CDT}$)

All specimens are from the Eschenbach-Bocksberg Quarry except for 9, which is from the Kreuzberg roof slate mine. Sample numbers correspond to those in app. 4.

SAMPLE NO.	FOSSIL				MATRIX (distance from fossil)		
					1-3cm	4-6cm	10-12cm
	ECHINODERMS						
1.	*Gastrocrinus* stem	+24.3 distal	+26.9 proximal		-15.5	-19.5	-23.1
2.	*Dicirrocrinus* stem	+22.3			+10.4	+5.4	-4.1
3.	crinoid indet. stem	-4.9			-17.4	-13.2	-17.0
4.	crinoid calyx	+6.1			+5.2	+9.6	+7.6
5.	asteroid indet.	+1.1			-11.7	-11.3	-10.8
	ARTHROPODS						
6.	*Chotecops*	+5.3 pygidium dorsal	+3.9 pygidium doublure	+3.3 limb	-25.7	-28.3	
7.	Trilobite indet.	+7.6 outer cephalon	+5.0 limbs		-14.5	-15.6	-9.6
8.	Trilobite unpyritized	-15.5			-11.3	-19.2	
9.	Trilobite unpyritized	-8.0			-11.5	-12.3	
10.	Trilobite unpyritized	+0.2			-12.9	+2.5	
11.	Trilobite unpyritized	-1.9			-7.1	-11.9	+12.3
12.	*Palaeoisopus*	-1.5			-24.0		
	ECHINODERMS AND ARTHROPODS ON THE SAME SLAB						
13.	asteroid indet.	+5.3			-21.6	-23.1	-22.1
	Palaeoisopus	-0.3					
14.	*Furcaster*	+10.4			-11.5 (3-4 cm from *Furcaster*)		
	Mimetaster	+12.6					

Appendix 2

Matrix samples associated with 10 fossils from areas of the Hunsrück Slate where pyritization does not occur: Fe data

Locality from which sample was obtained	% Fe		Potentially Reactive Fe/ Total Fe
	HCl	Total	
Kreuzberg	1.48	5.35	0.28
Kreuzberg	1.80	4.90	0.37
Kreuzberg	1.48	4.77	0.31
Kreuzberg	2.07	4.96	0.42
Kreuzberg	2.23	4.61	0.48
Maria Schacht	1.73	5.18	0.33
Maria Schacht	1.12	5.11	0.22
Margaretha	1.20	5.35	0.22
Margaretha	1.41	5.67	0.25
Kehrig	1.92	4.80	0.40

Appendix 3

Block: chemical and isotopic data

Values for Reactive Fe/Total Fe and DOP derived from pyrite sulfur where possible, otherwise from total sulfur.

Sample No.	Level above base (mm)	% Org C	% Sulfur		% Fe			Potentially reactive Fe/ Total Fe	$\delta^{34}S$‰	DOP
			Pyrite	Total	Dithionite	HCl	Total			
A2	124-145	0.33	0.09	-	0.08	0.71	5.74	0.14		0.10
A2/2	137-145								-24.7	-
A2/1	124-137			-					-20.7	-
A1	101-124	0.35	0.07	-	0.06	0.56	5.28	0.12	-16.5	0.10
B2	67-101	0.33	-	0.24	0.05	0.44	5.52	0.12	-	0.32
B1/2	84-101	0.28	0.09	-	0.05	0.44	5.47	0.10	-7.9	0.15
B1/1	67-84	-	0.08	-	-	-	-	-	-1.0	-
C2/2	51-67	0.31	-	0.23	0.09	1.15	5.52	0.24	-	0.15
C2/1	51-67	0.32	-	0.21	0.10	1.36	5.50	0.28	-	0.12
C2/0	51-67	0.32	0.13	0.19	0.08	1.31	5.56	0.27	-	0.08
C1/2	57-67	-		-	-	-	-	-	-14.4	-
C1/1	51-57	-	-	-	-	-	-	-	-14.3	-
D2/2	44-51	0.30	0.12	0.23	0.07	1.19	5.00	0.26	+2.4	0.08
D2/1 (lens depth)	37-44	0.45	-	0.35	0.06	1.44	5.25	0.33	+22.5	0.18
D1	28-37	-	0.72	-	-	-	-	-	+34.4	-
E	9-28	0.44	0.09	0.19	0.04	0.95	5.57	0.20	+5.8	0.08
F	0-9	-	0.08	-	0.05	0.82	5.39	0.17	+17.6	0.08
Lens edge	38-43	-	15.1	-	-	-	19.4	-	+7.1	-
Centre	38-43	-	29.4	-	-	-	27.2	-	+6.8	-
Lens edge	38-43	-	24.6	-	-	-	26.1	-	+7.5	-

APPENDIX 4

Matrix sediments: chemical data

Values for Reactive iron/Total iron and DOP derived from pyrite sulfur where possible, otherwise from total sulfur.

Sample no. and distance (cm) from fossil (see app. 1)	% Org C	%S		% Fe			Potentially reactive Fe/ Total Fe	DOP
		Pyrite	Total	Dithionite	HCl	Total		
1/1-3	0.30	0.17	0.14	0.06	1.40	5.42	0.29	0.10
1/4-6	0.26	0.16	0.13	0.07	2.19	5.36	0.43	0.06
1/10-12	0.25	0.20	0.12	0.11	1.07	5.60	0.22	0.14
2/1-3	0.28	0.14	0.34	0.15	2.65	5.42	0.51	0.04
2/4-6	0.26	0.13	0.21	0.15	1.57	5.43	0.31	0.07
2/10-12	0.40	-	0.21	0.14	2.17	5.54	0.42	0.08
3/1-3	-	0.14	0.13	0.14	3.54	5.84	0.63	0.03
3/4-6	-	0.12	0.14	0.13	2.98	5.84	0.53	0.03
3/10-12	-	0.12	0.22	0.23	3.66	5.77	0.65	0.03
4/1-3	0.33	0.06	0.12	0.11	2.88	5.47	0.54	0.02
4/4-6	-	0.08	0.11	0.15	3.41	5.65	0.62	0.02
4/10-12	-	0.14	0.24	-	-	-	-	-
5/1-3	-	0.09	0.20	-	-	-	-	-
5/4-6	-	0.06	-	0.16	2.95	5.76	0.52	0.02
5/10-12	-	0.09	0.14	0.29	3.31	-	-	0.02
6/1-3	0.38	-	0.15	0.03	2.42	6.33	0.40	0.05
6/4-6	0.40	0.16	0.12	0.05	1.07	6.43	0.19	0.12
7	-	0.27	0.26	0.24	-	5.50	-	-
8/1-3	0.54	-	0.53	0.11	3.32	5.69	0.66	0.12
8/4-6	0.52	0.17	0.22	0.07	2.66	5.33	0.53	0.05
9/1-3	-	0.06	-	-	-	4.84	-	-
9/4-6	-	0.01	-	-	-	4.65	-	-
10/1-3	-	0.05	-	-	-	5.63	-	-
10/4-6	-	0.07	-	-	-	5.58	-	-
11/1-3	-	0.09	-	-	-	5.52	-	-
11/4-6	-	0.06	-	-	-	5.51	-	-
11/10-12	-	0.12	-	-	-	5.60	-	-
12/1-3	0.35	-	0.20	0.09	3.18	5.77	0.58	0.05
13/1-3	0.37	-	0.18	0.06	1.64	5.84	0.31	0.09
13/4-6	0.36	-	0.28	0.06	0.99	5.83	0.21	0.20
13/10-12	0.38	-	0.11	0.06	2.13	5.99	0.37	0.04
14/3-4	0.36	-	0.09	0.33	3.86	5.65	0.70	0.02

REFERENCES

Aller, R. C., Mackin, J. E. and Cox, R. T., Jr., 1986, Diagenesis of Fe and S in Amazon Inner Shelf muds: Apparent dominance of Fe reduction and implications for the genesis of ironstones: Continental Shelf Research, v. 6, p. 263–289.

Allison, P. A., 1988, *Konservat-Lagerstätten:* cause and classification: Paleobiology, v. 14, p. 331–344.

Allison, P. A., and Briggs, D. E. G., 1991. Taphonomy of non-mineralized tissues, in Allison, P. A., and Briggs, D. E. G., editors, Taphonomy: Releasing the data locked in the fossil record: New York, Plenum Press, p. 25–69.

Baas, M., Briggs, D. E. G., van Heemst, J. D. H., Kear, A. J., and de Leeuw, J. W., 1995, Selective preservation of chitin during the decay of shrimp: Geochimica et Cosmochimica Acta, v. 59, p. 945–951.

Bartels, C., and Blind, W., 1995, Röntgenuntersuchung pyritisch vererzter Fossilien aus dem Hunsrückschiefer (Unter-Devon, Rheinisches Schiefergebirge): Metalla, Forschungsberichte des Deutschen Bergbau-Museums, v. 2, p. 79–100.

Bartels, C., and Brassel, G., 1990, Fossilien im Hunsrückschiefer—Dokumente des Meereslebens im Devon: Idar-Oberstein, Museum Idar-Oberstein, 232 p.

Bartels, C., and Wuttke, M., 1994a, Fossil Überlieferung von Weichkörperstruckturen und ihre Genese im Hunsrückschiefer (Unter-Ems, Rheinisches Schiefergebirge): ein Forschungsbericht: Giessener Geologische Schriften, v. 51, p. 25–61.

——— 1994b, Nachtrag zu: Fossil Überlieferung von Weichkörperstruckturen und ihre Genese im Hunsrückschiefer (Unter-Ems, Rheinisches Schiefergebirge): ein Forschungsbericht: Giessener Geologische Schriften, v. 51, p. 329–333.

Beier, J. A., and Feldman, H. R., 1991, Sulfur isotopes and paragenesis of sulfide minerals in the Silurian Waldron Shale, southern Indiana: Geology, v. 19, p. 389–392.

Berner, R. A., 1964, Distribution and diagenesis of sulfur in some sediments from the Gulf of California: Marine Geology, v. 1, p. 117–140.

——— 1970, Sedimentary pyrite formation: American Journal of Science, v. 268, p. 1–23.

——— 1984, Sedimentary pyrite formation: an update: Geochimica Cosmochimica Acta, v. 48, p. 605–615.

Boudreau, B. P., and Canfield, D. E., 1988, A provisional diagenetic model for pH in anoxic porewaters: Journal of Marine Research, v. 46, p. 429–455.

Brett, C. E., and Baird, G. C., 1986, Comparative taphonomy: a key to paleoenvironmental interpretation based on fossil preservation: Palaios, v. 1, p. 207–227.

Briggs, D. E. G., 1991, Extraordinary fossils: American Scientist, v. 79, p. 130–141.

Briggs, D. E. G., Bottrell, S. H., and Raiswell, R., 1991, Pyritization of soft-bodied fossils: Beecher's Trilobite Bed, Upper Ordovician, New York State: Geology, v. 19, p. 1221–1224.

Briggs, D. E. G., and Edgecombe, G., 1992, The gold bugs: Natural History, v. 92/11, p. 36–43.

——— 1993, Beecher's Trilobite Bed: Geology Today, v. 9, p. 97–102.

Briggs, D. E. G., and Kear, A. J., 1993, Fossilisation of soft-tissue in the laboratory: Science, v. 259, p. 1439–1442.

Briggs, D. E. G., Kear, A. J., Baas, M., de Leeuw, J. W., and Rigby, S., 1995, Decay and composition of the hemichordate *Rhabdopleura:* implications for the taphonomy of graptolites: Lethaia v. 28, p. 15–23.

Briggs, D. E. G., Kear, A. J., Martill, D. M., and Wilby, P. R., 1993, Phosphatization of soft-tissue in experiments and fossils: Journal of the Geological Society, London, v. 150, p. 1035–1038.

Bromley, R. G., and Ekdale, A. A., 1984, *Chondrites:* a trace fossil indicator of anoxia in sediments: Science, v. 224, p. 872–874.

Canfield, D. E., 1989, Reactive iron in marine sediments: Geochimica Cosmochimica Acta, v. 53, p. 619–632.

Canfield, D. E., and Raiswell, R., 1991, Pyrite formation and fossil preservation, in Allison, P. A., and Briggs, D. E. G., editors, Taphonomy: Releasing the data locked in the fossil record: New York, Plenum Press, p. 337–387.

Canfield, D. E., Raiswell, R., and Bottrell, S. H., 1992, The reactivity of sedimentary iron minerals towards sulfide: American Journal of Science, v. 292, p. 659–683.

Canfield, D. E., Raiswell, R., Westrich, J. T., Reaves, C. M., and Berner, R. A., 1986, The use of chromium reduction in the analysis of reduced inorganic sulfur in sediments and shales: Chemical Geology, v. 54, p. 149–155.

Chambers, L. A., and Trudinger, P. A., 1979, Microbiological fractionation of stable sulfur isotopes: a review and critique: Geomicrobiological Journal, v. 1, p. 249–293.

Cisne, J. L., 1973, Beecher's Trilobite Bed revisited: Ecology of an Ordovician deepwater fauna: Postilla, v. 160, 25 p.
Claypool, G. E., Holser, W. T., Kaplan, I. R., Sakai, H., and Zak, I., 1980, The age curves for sulfur and oxygen isotopes in marine sulfate and their mutual interpretation: Chemical Geology, v. 28, p. 199–260.
Coleman, M. L., and Raiswell, R., 1995, Source of carbonate and origin of zonation in pyritiferous carbonate concretions: evaluation of a dynamic model: American Journal of Science, v. 295, p. 282–308.
Dittmar, U., ms, 1995, Profilbilanzierung und Verformungsanalyse in südwestlichen Rheinischen Schiefergebirge. Zur Konfiguration, Deformation und Entwicklungsgeschichte eines passiven varistischen Kontinentalrandes: Doctoral dissertation, Julius-Maximilians-Universität, Würzburg, 461 p.
Fisher, I. St J., and Hudson, J. D., 1985, Pyrite geochemistry and fossil preservation in shales: Philosophical Transactions of the Royal Society of London B, v. 311, p. 167–169.
Goldhaber, M. B. and Kaplan, I. R., 1974, The sulfur cycle, in Goldberg, E. D., editor, The Sea, Volume 5: Wiley-Interscience, p. 569–655.
Hall, A. J., Boyce, A. J., and Fallick, A. E., 1987, Iron sulphides in metasediments: isotopic support for a retrogressive pyrrhotite to pyrite reaction: Chemical Geology, v. 65, p. 305–310.
———— 1994, A sulphur isotope study of iron sulphides in the late Precambrian Dalradian Ardrishaig Phyllite Formation, Knapdale, Argyll: Scottish Journal of Geology, v. 30, p. 63–71.
Hof, C., and Briggs, D. E. G., 1997, Decay and mineralization of mantis shrimps (Stomatopoda: Crustacea): Palaios, in review.
Howarth, R. W., 1979, Pyrite: its rapid formation in a salt marsh and its importance in ecosystem metabolism: Science, v. 203, p. 49–51.
Hudson, J. D., 1982, Pyrite in ammonite-bearing shales from the Jurassic of England and Germany: Sedimentology, v. 29, p. 639–667.
Kaplan, I. R., and Rittenberg, S. C., 1964, Microbiological fractionation of sulphur isotopes: Journal of General Microbiology, v. 34, p. 195–212.
Kott, R., and Wuttke, M., 1987, Untersuchungen zur Morphologie, Paläökologie und Taphonomie von *Retifungus rudens* Rietschel 1970 aus dem Hunsrückschiefer (Bundesrepublik Deutschland): Geologisches Jahrbuch Hessen, v. 115, p. 11–27.
Martill, D. M., 1990, Macromolecular resolution of fossilized muscle tissues from an elopomorph fish: Nature, v. 346, p. 171–172.
Middelburg, J. J., 1989, A simple rate model for organic matter decompositions in marine sediments: Geochimica Cosmochimica Acta, v. 53, p. 1577–1581.
Mittmeyer, H.-G., 1980, Zur geologie des Hunsrückschiefers: Veresteinertes Leben im Röntgenlicht: Kleine Senckenberg Reihe, v. 11, p. 26–33.
Murowchick, J. B., and Barnes, H. L., 1987, Effects of temperature and degree of supersaturation on pyrite morphology: American Mineralogist, v. 72, p. 1241–1250.
Nakai, N., and Jensen, M. L., 1964, The kinetic isotope effect in the bacterial reduction and oxidation of sulfur: Geochimica Cosmochimica Acta, v. 28, p. 1893–1912.
Newton, R. J., Bottrell, S. H., Dean, S. P., Hatfield, D., and Raiswell, R., 1995, An evaluation of the use of the chromous chloride reduction method for isotopic analyses of pyrite in rocks and sediment: Chemical Geology, v. 125, p. 317–320.
Otto, M., 1994, Zur frage der 'Weichteilerhaltung" im Hunsrückschiefer: Geologica et Palaeontologica, v. 28, p. 45–63.
Raiswell, R., and Al-Biatty, H. J., 1989, Depositional and diagenetic C-S-Fe signatures in early Paleozoic normal marine shales: Geochimica Cosmochimica Acta, v. 53, p. 1147–1152.
———— 1992, Depositional and diagenetic C-S-Fe signatures and the potential of shales to generate metal-rich fluids, in Schidlowski, M., editor, Early Organic Evolution: Implications for Mineral and Energy Resources: Springer-Verlag, Berlin, p. 415–425.
Raiswell, R., and Berner, R. A., 1986, Pyrite and organic matter in Phanerozoic normal marine shales: Geochimica Cosmochimica Acta, v. 50, p. 1967–1976.
———— 1987, Organic carbon losses during burial and thermal maturation of normal marine shales: Geology, v. 15, p. 853–856.
Raiswell, R., Buckley, F., Berner, R. A., and Anderson, T. F., 1988, Degree of pyritization of iron as a paleoenvironmental indicator of bottom water oxygenation: Journal of Sedimentary Petrology, v. 58, p. 812–819.
Raiswell, R., Canfield, D. E., and Berner, R. A., 1994, A comparison of iron extraction methods for the determination of degree of pyritization and the recognition of iron-limited pyrite formation: Chemical Geology, v. 111, p. 101–110.

Raiswell, R., Whaler, K., Dean, S., Coleman, M. L., and Briggs, D. E. G., 1993, A simple three-dimensional diffusion-plus-precipitation model applied to localized pyrite formation in framboids, fossils and detrital iron minerals: Marine Geology, v. 113, p. 89–100.
Rickard, D. T., 1975, Kinetics and mechanisms of pyrite formation at low temperatures: American Journal of Science, v. 275, p. 636–652.
Rickard, D. T., Schoonen, M. A. A., and Luther, G. W. III, 1995, The chemistry of iron sulfides in sedimentary environments, *in* Vairavamurthy, V., and Schooner, M. A. A., editors, Geochemical Transformations of Sedimentary Sulfur, American Chemical Society Symposium Series, v. 612, p. 168–193.
Robinson, B. W., and Kusakabe, M., 1975, Quantitative preparation of sulfur dioxide for $^{34}S/^{32}S$ analyses, from sulfides by combustion with cuprous oxide: Analytical Chemistry, v. 47, p. 1179–1181.
Ronov, A. B., and Migdisov, A. A., 1971, Geochemical history of the crystalline basement and the sedimentary cover of the Russian and North American platforms: Sedimentology, v. 16, p. 137–185.
Roy, A. S., 1978, Evolution of slaty cleavage in relation to diagenesis and metamorphism: a study from the Hunsrückschiefer: Geological Society of America Bulletin, v. 89, 1775–1785.
Schoonen, M. A. A., and Barnes, H. L., 1991a, Reactions forming pyrite and marcasite from solution. I Nucleation of FeS_2 below 100°C: Geochimica Cosmochimica Acta, v. 55, p. 1495–1504.
———— 1991b, Reactions forming pyrite and marcasite from solution. II Via FeS precursors below 100°C: Geochimica Cosmochimica Acta, v. 55, p. 1505–1514.
Stürmer, W., 1985, A small coleoid cephalopod with soft parts from the Lower Devonian discovered using radiography: Nature, v. 318, p. 53–55.
Stürmer, W., and Bergström, J., 1973, New discoveries on trilobites by X-rays: Paläontologische Zeitschrift, v. 47, p. 104–141.
Stürmer, W., Schaarschmidt, F., and Mittmeyer, H.-G., 1980, Veresteinertes Leben im Röntgenlicht: Kleine Senckenberg Reihe, v. 11, 80 p.
Talbot, J. L., 1964, Crenulation cleavage in the Hunsrückschiefer of the Middle Moselle region: Geologische Rundschau, v. 54, 1026–1043.
Westrich, J. T., and Berner, R. A., 1984, The role of sedimentary organic matter in bacterial sulfate reduction: The G model tested: Limnology and Oceanography, v. 29, p. 236–249.
Wilby, P. R., Briggs, D. E. G. and Riou, B., 1996, Mineralization of soft bodied invertebrates in a Jurassic metalliferous deposit: Geology, in review.